IEEE Open Journal of
Antennas and Propagation

Received 6 June 2020; revised 15 July 2020; accepted 20 July 2020. Date of publication 27 July 2020; date of current version 11 August 2020.

Digital Object Identifier 10.1109/OJAP.2020.3011920

Novel Time-Domain Electromagnetic Simulation Using Triangular Meshes by Applying Space Curvature

M. R. KAZEMZADEH [1], N. G. R. BRODERICK [2], AND W. XU [1] (Senior Member, IEEE)

[1]Department of Mechanical Engineering, University of Auckland, Auckland 1010, New Zealand

[2]Dodd-Walls Centre, Photon Factory, Department of Physics, University of Auckland, Auckland 1010, New Zealand

CORRESPONDING AUTHOR: M. R. KAZEMZADEH (e-mail: mkaz499@aucklanduni.ac.nz)

This work was supported in part by the Dodd-Walls Centre for Photonic and Quantum Technologies, and in part by the Goodfellow Fund for Support of Urological Research, New Zealand.

ABSTRACT A novel stable, accurate and fast numerical method based on triangular meshing and space transformations for electrodynamics problems with arbitrary boundaries is developed. Using transformation optics it is possible to convert non uniform domains into uniform rectangular ones allowing Maxwell's Equations to be solved quickly and simply using a modified finite difference time domain (FDTD) algorithm. A novel averaging method is presented to ensure the stability and accuracy of our algorithm when dealing with anisotropic and inhomogeneous materials in the transformed space. Finally we demonstrate the advantages of the present technique compared with conventional FDTD and transformation optics FDTD through a couple of scattering problems. These show that this method is more than one thousand times faster than classical FDTD in the presence of curved boundaries.

INDEX TERMS Numerical analysis, computational optics, FDTD.

I. INTRODUCTION

THE FINITE-DIFFERENCE time-domain (FDTD) [1]–[4] algorithm is a widely used numerical method for modelling a wide range of electromagnetic problems. It is often used to model optical systems due to its time-domain approach making it ideal for finding the frequency response and for investigating the non-linear behaviour of different systems. Despite its relatively easier implementation compared to another numerical method such as the finite element method, it suffers from numerical instability and relatively larger numerical errors since it is a second-order centred finite difference method in time and space.

The conventional FDTD algorithm solves Maxwell's equations by using a second-order centred finite difference approximation of the field's derivatives which requires a uniform rectangular grid over the entire simulation window with a typical grid spacing of $\lambda/10$ to ensure convergence and accuracy. This meshing uniformity and high density becomes very problematic especially when we are dealing with isolated subwavelength geometrical details in a relatively large computational domain as it forces the whole meshing grid to be small enough to take the small details into the account. Similarly a uniform mesh results in a geometrical discretization error when dealing with curved boundaries or interfaces between materials. Various algorithms such as sub-gridding FDTD and adaptive mesh refinement (AMR) [5]–[14] try to address these problems by considering a local area with smaller grid sizes but this can lead to the well known late time instability [13]–[17] due to its spatial and temporal interpolations and such approaches usually cannot avoid the geometric discretization error. Another problem of these approaches is higher amount of error when the ratio of spatial steps becomes large. The Huygens sub-griding method [13], [14] solves this issue but it still suffers from late-time instability.

Recently space transformations have been widely used to handle meshing problems in finite difference and finite element numerical approaches. Quadrilateral gridding for solving partial differential equations [18]–[20], curvilinear FDTD [21], [22] and nonorthogonal grid FDTD [23], [24] are methods that applied space transformation to deal with geometrical discontinuity and uniformity of finite difference

meshing. However, these transformations change their target partial differential equations (Maxwell's equations in case of FDTD). Therefore, some consequences such as nonphysical, non-divergence-free and late-time unstable solutions have been encountered [25].

It is however possible to ensure that the solutions of the transformed equations map one to one onto the solutions of the real physical system provided that in addition to transforming the spatial grid the material parameters are also changed appropriately [26]–[30]. This approach takes concepts from transformation optics [31] and uses them to solve Maxwell's Equations over an arbitrary domain and such methods are known as TO-FDTD. The idea is to find a set of transformations for both space and the local material properties that leave Maxwell's equations invariant so that a solution in the transformed space is easy to find numerically (or analytically) and then this solution can be transformed using the inverse transformation back into real space. While in principle this method (TO-FDTD) can solve all of the above issues with FDTD it brings its own set of problems relating to the highly non-uniform and anisotropic material parameters (ε and μ) in the transformed system.

Anisotropic materials can lead to numerical instability in classical FDTD algorithms depending on the chosen grid and interpolation procedure. However methods have been developed that can avoid these instabilities by correctly averaging the material across different cells [32]–[34]. Moreover, the small relative permittivity and permeability can also create numerical instability for an explicit FDTD algorithm, as the speed of wave propagation increases with decreased relative permittivity and permeability. In fact, a wave must not propagate further than a single unit cell per time step in explicit discrete-time simulations. This constraint is known as Courant-Friedrichs-Lewy stability condition [35] for hyperbolic partial differential equations. In [26]–[30] dispersive materials were used to ensure numerical stability. However, using such dispersive materials add unwanted frequency dependencies to the simulation making it harder to simulate conditions across a broad frequency range.

In addition to all of the previously mentioned problems for transformation optics FDTD methods, these methods typically involve extra analytical or numerical effort to find the optimal transformations. These transformations are finely tuned based on the given problems' geometry so if we want to change any geometrical parameters we need start again at the very beginning of the process. This lack of robustness makes current transformation optics FDTD algorithms impractical for optimization problems where we want to find the best geometry for example. Moreover, none of the transformation optics FDTD methods consider their transformation in the sense of avoiding staircase error [36].

In this work, we present a novel triangular FDTD meshing scheme that firstly minimises the discretization error from all the internal and external boundaries and secondly provides us with total freedom over the mesh density in the vicinity of any number arbitrary points or area of the simulation window. Then, based on these obtained meshes, a new virtual space will be generated with a uniform grid. Then we present a new method for the implementation of an unconditionally stable explicit FDTD for inhomogeneous anisotropic materials without adding unwanted frequency dependency for the proposed triangular meshing scheme. After solving the problem in transformed uniform space we bring back the results into our initial space. Finally the superiority of the present method against classical FDTD and transformation optic FDTD is shown using a couple of examples.

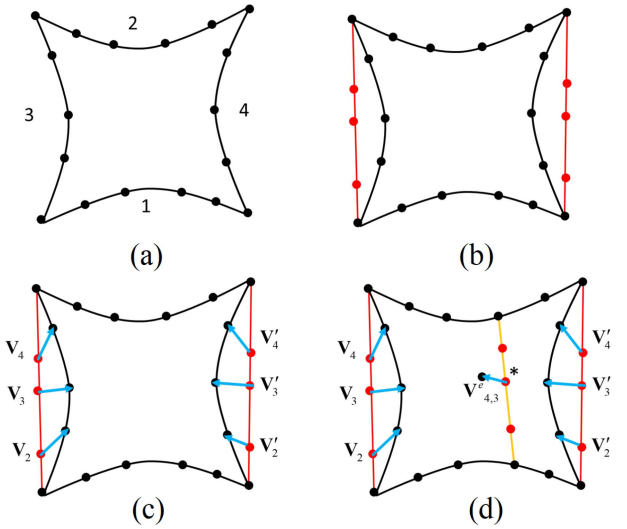

FIGURE 1. (a) Allocating an equal number of points on the edges (one and two) and (three and four). (b) drawing a line between the first and last points of edges one and two of (a) and dividing it by the equal number of points on edges three and four. (c) calculation of displacement vectors. (d) calculation of effective displacement vectors based on the location of internal meshing points.

II. METHODOLOGY

Our ultimate aim is to find a transformation that converts an arbitrary shaped region of the plane into a rectangle on which we can solve Maxwell's equations quickly and efficiently using the FDTD algorithm (the extension to a fully 3D simulation is relatively straightforward but computationally much more extensive so is not considered here). Since we are dealing with a numerical approach we need only consider the transformation at the desired grid points which can be chosen to avoid both staircase errors and late time instabilities or inaccuracies. Whilst in the literature there is a significant body of work on algorithmically generating grid points most of this is concerned with triangular meshes suitable for finite element simulations and to the best of our knowledge no algorithm for generating grid points suitable for use in transformation optics has been explicitly presented before. Thus we first present our gridding algorithm before discussing its applicability in FDTD simulations.

A. MESHING METHOD

We firstly have to generate a mesh based on the given interior and exterior boundaries of the scenario. For the sake

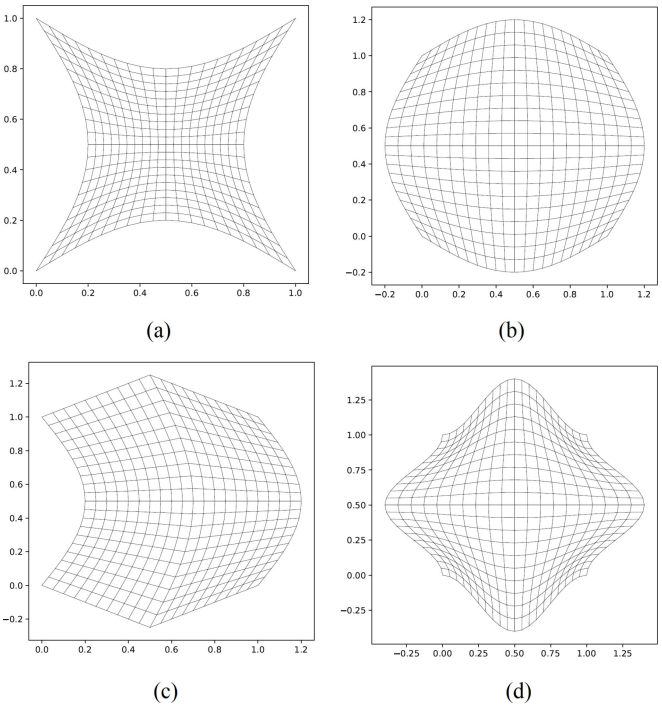

FIGURE 2. Meshing example using the proposed method.

of simplicity, consider a system with only exterior boundaries as illustrated in Fig. 1(a) with the grid points on the boundary are indicated by the solid dots. These points must be chosen such that there are N points along the top and bottom boundaries while there can be M points along the left and right edges (with the ultimate aim of producing a uniform rectangular $N \times M$ grid in the transformed space).

The next step is to start with two vertical lines connecting the left and right sides of the boundaries as shown in Fig. 1(b). Along each vertical line we add at M arbitrary locations grid points (shown in red). The location of these points will be chosen to maximise the grid density where needed. We can then define two functions f_l and f_r that map the i^{th} vertical grid point to the i^{th} grid point of the curved boundary as shown in Fig. 1(c). Using these functions we can define the displacement vectors $\delta\mathbf{v}_i^l$ and $\delta\mathbf{v}_i^r$ by

$$\delta\mathbf{v}_i^l = f_l(\mathbf{v}_i) - \mathbf{v}_i \quad \text{and} \quad \delta\mathbf{v}_i^r = f_r(\mathbf{v'}_i) - \mathbf{v'}_i \tag{1}$$

Then we wish to choose interior grid points such that the resulting grid lines smoothly map from one boundary to another. We start by drawing a straight line between the ith grid point along the top boundary and the ith grid point along the bottom boundary. And we add in M grid points along this line as shown in Fig. 1(d). The j grid point on this line $\mathbf{v}_{i,j}$ is then displaced by the weighted sum of the displacement vectors $\delta\mathbf{v}_i^l$ and $\delta\mathbf{v}_i^r$, i.e.,

$$\mathbf{v}^e{}_{i,j} = \mathbf{v}_{i,j} + \frac{i\delta\mathbf{v}_j^r + (N-i)\delta\mathbf{v}_j^l}{N} \tag{2}$$

Note that Eq. (2) can shift interior points outside the boundary in which case, we must change the location of the initial points [i.e., either the edge points or the points that we assigned on the lines between the edge points Fig. 1(d)] to make sure that the transformed point lies in the interior. Examples of generated meshes based on the above technique for different exterior boundaries are presented in Fig. 2. (a), (b), (c) and (d). For all of these examples, all the assigned points on all edges and generated lines chose to be uniformly distributed. As can be seen in these figures, the geometrical behaviour of exterior boundaries has been kept in all of the meshes.

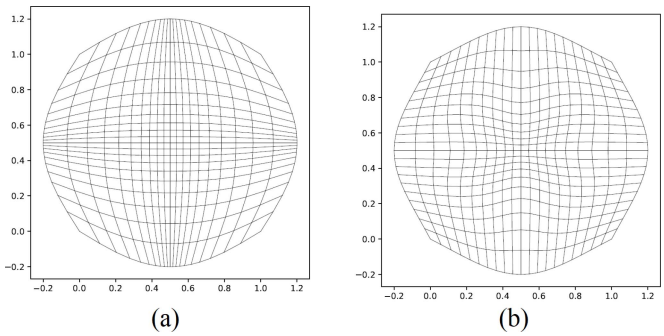

FIGURE 3. Increasing the number of meshing cells in the center (a) using changing the distribution of meshing points in the boundary (b) by changing the effective vector.

Using this approach there is still considerable freedom to chose the meshing function that allows us to alter the density of the mesh in specific regions (we will need this to deal with curved boundaries and small scale features when solving Maxwell's equations). We can propose two ways that let us chose the density of the meshing points in the specific area within the meshing domain. The first way, shown in Fig. 3(a), is to change the distribution of the assigned points in the edges and the second approach is changing the distribution of the interior points along specific lines as shown in Fig. 3(b). In the first approach, we can see there are more distortions in meshing grids than the second approach. We thus adopt the second approach in this work since it leads to better results for our FDTD simulations.

1) MORE COMPLEX GEOMETRIES

The method outlined above handles simple geometries very easily but fails for more complicated shapes or for waveguides with internal boundaries such as the one shown in Fig. 4(a). To handle the internal boundary for meshing using the proposed method this structure should be divided into three sections which are the two blue and the one red section in Fig. 4(a). Then, each part can be meshed independently as shown in Fig. 4(b), using the original method. The only constraint for the meshing in each section is that the distribution and the location of the meshing points on each internal boundaries must be the same for the adjacent sections. This is essential as the whole mesh must eventually be transformed into a uniform grid. Similarly more complicated geometries can all be split into simple regions and meshed accordingly.

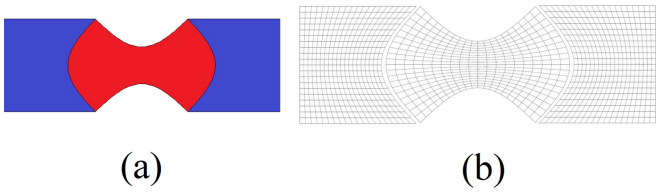

FIGURE 4. (a) arbitrary geometry with internal boundaries. (b) resulted mesh.

B. CALCULATION OF MATERIAL PROPERTIES OF EACH MESHING CELL

Solving Maxwell's equations using the FDTD method, works best in terms of numerical stability and accuracy when done on a uniform grid [26], [30]. For this reason, we want to transform our more general meshing scheme to a uniform rectangular grid then we can solve the problem in the transformed space using FDTD. To achieve this we can find a transformation for each meshing cell and find the appropriate change of material property based on the obtained transformation. Consider a general three-dimensional transformation $\mathbf{T} : \mathbb{R}^3 \Rightarrow \mathbb{R}^3$. This transformation must be locally invertible so we will be able to transform the solution back into the initial space. Furthermore as each meshing cell must be chosen to be significantly smaller than the local wavelength (typically smaller than 1/10 of wavelength), we can approximate $\mathbf{T}$ as a linear transformation valid over each cell. Such an approximation is necessary for the FDTD algorithm since we need to specify the material properties at each grid point. Therefore, we can rewrite our general transformation as:

$$\mathbf{T}(\mathbf{x}_0 + \delta\mathbf{x}) = \mathbf{T}(\mathbf{x}_0) + \Lambda\delta\mathbf{x} \tag{3}$$

in which Λ is the Jacobean matrix of the transformation. $\mathbf{x}_0$ and $\delta\mathbf{x}$ are an arbitrary point and small deviation from it, respectively. In our case $\mathbf{T}$ is defined by the requirement that a grid point $\mathbf{x}_{i,j}$ in real space gets transformed to the regular grid point $(i\Delta x', j\Delta y')$, in which $\Delta x'$ and $\Delta y'$ represent the width and height of each cell in virtual space grid, in the transformed space and furthermore the tangent vectors to the grid lines in real space become orthogonal at each grid point in the transformed space. Note that in general $\mathbf{T}$ and Λ will vary from point to point and as we will see this causes issues with the stability of the FDTD algorithm as discussed below.

Given the transformation $\mathbf{T}$ defined locally by Eq. (3) we can find a solution to Maxwell's equations in the transformed space that is completely equivalent to the real space solution provided that the optical path length between any two points remains the same. It can be shown that if distances are altered via Eq. (3) then this requires that the relative permittivity and permeability transform as:

$$\varepsilon^{tr} = \frac{\Lambda\varepsilon\Lambda^T}{\det(\Lambda)} \tag{4a}$$

$$\mu^{tr} = \frac{\Lambda\mu\Lambda^T}{\det(\Lambda)} \tag{4b}$$

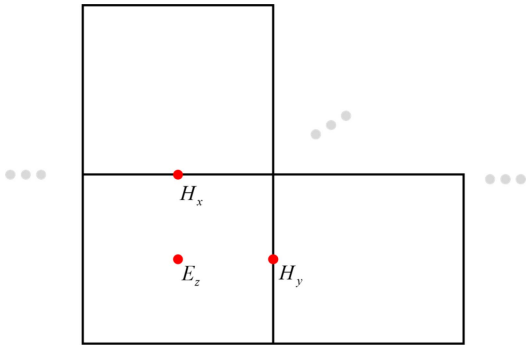

FIGURE 5. Standard Yee cell and the location of the points where the electric and magnetic fields are calculated.

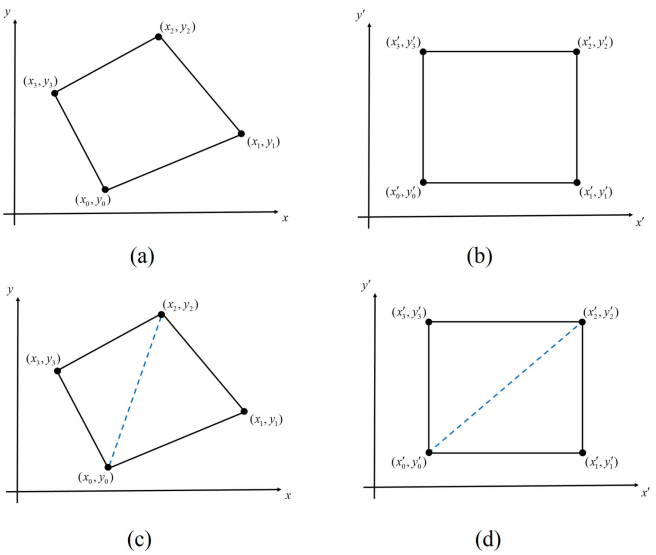

FIGURE 6. (a) and (b) arbitrary meshing cell in initial and transformed space. (c) and (d) deviation of meshing cell into two triangles in initial and transformed space.

in which ε, μ, ε^{tr}, and μ^{tr} are permittivity and permeability in initial and transformed space, respectively. Note that ε^{tr} and μ^{tr} are now anisotropic and are also spatially varying even if the original material was uniform. Both of these raise issues with the standard FDTD algorithm due to the non hermitian nature of the standard discretization of space. This is illustrated in Fig. 5 which shows the standard Yee cell for the FDTD algorithm. As can be seen the electric and magnetic fields are evaluated at different points in space and thus ε^{tr} and μ^{tr} will also be evaluated at different spatial points. Numerically this means that the difference equations approximating Maxwell's equations are non-hermitian and thus exponentially increasing solutions can occur leading to the onset of late time instabilities. In the next section we show how this can be avoided and then demonstrate this using some examples.

To see how these anisotropies arise we consider in detail the transformation of a single mesh cell in real space to a rectangle in the transformed space. This is shown in Fig. 6 (a) and (b). Note that as a rectangle has 4 corners while a linear transformation in 2D has only two degrees of freedom it is not possible to find a linear transformation that does

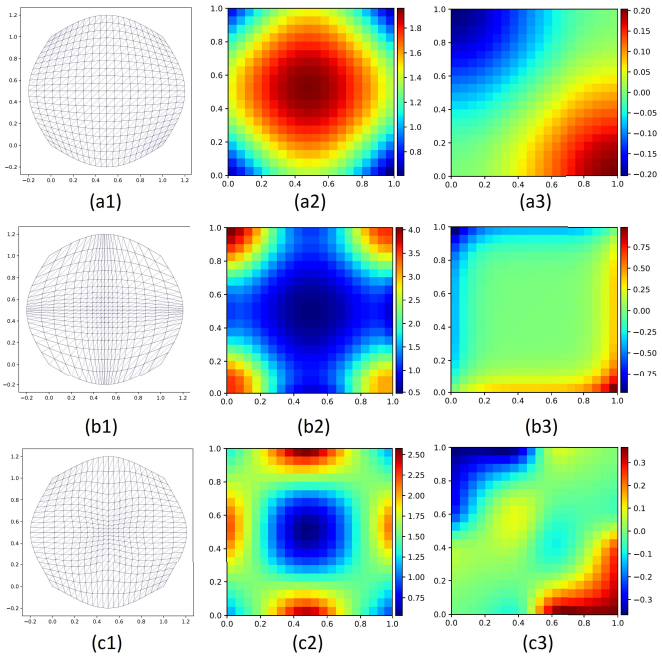

FIGURE 7. (a1), (b1) and (c1) triangular meshing. (a2), (b2) and (c2) ε_{zz}^{tr} distribution corresponding to the lower triangle in each mesh cell of (a1), (b1) and (c1), respectively. (a3), (b3) and (c3) differences between the value of ε_{zz}^{tr} for upper and lower triangle related to meshes in (a1), (b1) and (c1), respectively.

such a mapping. Instead we need two linear transformations, one for each of the triangles in Fig. 6 (c). So by Eq. (4) the material properties are different in the upper and lower half of each grid cell. In particular note that in the FDTD algorithm E_z is calculated in the middle of each grid cell which is where ε^{tr} is discontinuous and thus we need to modify the FDTD algorithm to take this into account.

Finally as an explicit example of how the material properties change with the gridding we show in Fig. 7 three different meshes [(a1), (b1), (c1)] for the same shape. Mesh (a1) has the greatest density of cells near the edges while mesh (b1) has more cells in the middle of both the vertical and horizontal directions while mesh (c1) has the most mesh cells in the centre. In all cases the original value of $\varepsilon = 1$ corresponding to empty space. Figs. 7(a2),(b2),(c2) show the calculated ε^{tr} for the lower half cells in the transformed uniform grid according to Eq. (4). Note that where the mesh points are further away, the speed of light in the transformed space decreases, (ε^{tr}) increases, while where the density of points increases the speed of light in transformed space increases, (ε^{tr}) decreases, so when going back to the real space light travels at the same speed everywhere. Finally the difference between ε^{tr} in the upper and lower triangles for each grid cell is shown in Figs. 7(a3),(b3),(c3). In all cases although the difference is small it is enough to cause instabilities in the FDTD algorithm as discussed below.

C. IMPLEMENTATION OF A STABLE FDTD ALGORITHM FOR ANISOTROPIC MEDIA USING A TRIANGULAR MESH

As we want to solve Maxwell's equations in the transformed space, we need to focus on the numerical solution for a uniform grid. Let's first find the stability condition for FDTD in the presence of anisotropic media. The relevant Maxwell equations are as:

$$\nabla \times \mathbf{E} = -\mu^{\mathbf{tr}} \frac{\partial \mathbf{H}}{\partial t} \tag{5a}$$

$$\nabla \times \mathbf{H} = \varepsilon^{tr} \frac{\partial \mathbf{E}}{\partial t} \tag{5b}$$

in which $\mathbf{E}$ and $\mathbf{H}$ are electric and magnetic fields, respectively. We can combine these equations into a single one as:

$$\nabla \times \left(\varepsilon^{tr^{-1}} \nabla \times \mathbf{H}\right) = -\mu^{tr} \frac{\partial^2 \mathbf{H}}{\partial\, t^2} \tag{6}$$

For non-magnetic materials the relative permeability is unity so inserting Eq. (4b) in Eq. (6) gives

$$\nabla \times \left(\varepsilon^{tr^{-1}} \nabla \times \mathbf{H}\right) = -\frac{\Lambda \Lambda^T}{\det(\Lambda)} \frac{\partial^2 \mathbf{H}}{\partial\, t^2} \tag{7}$$

Since Λ is not a function of time we can rewrite Eq. (7) as

$$\Lambda^{-1} \nabla \times \varepsilon^{tr^{-1}} \nabla \times \Lambda^{T^{-1}} \left(\Lambda^T \mathbf{H}\right) = -\frac{1}{\det(\Lambda)} \frac{\partial^2}{\partial t^2} \left(\Lambda^T \mathbf{H}\right) \tag{8}$$

Eq. (8) is a eigenvalue equation for the new variable $\Lambda^T \mathbf{H}$ which is an eigenvector of the operator $\mathbb{O} = \Lambda^{-1} \nabla \times \varepsilon^{tr^{-1}} \nabla \times \Lambda^{T^{-1}}$. It can be shown that the operator $\mathbb{O}$ is Hermitian since all of the operators involved are, including $\varepsilon^{tr^{-1}}$ which is the only non-trivial case. From Eq. (4a) we can see that ε^{tr} is Hermitian since ε is symmetric (assuming lossless media) and thus so is $\varepsilon^{tr^{-1}}$ since the inverse of a Hermitian matrix is also Hermitian. Returning to Eq. (8) we see that all of the eigenvalues of $\mathbb{O}$ are real and so the solutions are complex exponentials and hence as expected no solutions will grow exponentially in time.

In order to construct an unconditionally stable numerical algorithm we thus need to find a discrete Hermitian counterpart to $\mathbb{O}$ that is defined using the standard Yee cells. Previously Werner and Cary proposed a stable FDTD algorithm for solving Maxwell's equations involving non-diagonal and anisotropic dielectrics [32] and this approach can be easily extended to our case. The key to their approach came from recognising that the standard FDTD algorithm evaluates the electric and magnetic fields at different points in space [see Fig. 5] and an interpolation procedure is needed to create second order accurate centred difference approximations to the material parameters. This procedure results in the discretised eigenvalue equation

$$\Lambda^{-1} \left[\nabla^+ \times\right] \varepsilon^{tr^{-1}} \left[\nabla^- \times\right] \Lambda^{T^{-1}} \left(\Lambda^T \mathbf{H}\right) = -\frac{1}{\det(\Lambda)} \frac{\partial^2 \Lambda^T \mathbf{H}}{\partial t^2} \tag{9}$$

where the forward and backward curl operators ($\nabla^{\pm}$) are defined in [32, eq. (13)]. Eq. (9) is still an eigenvalue equation but for the discrete operator $\mathbb{O}_d$. Importantly $\mathbb{O}_d$ is Hermitian as long as the discrete version of $(\varepsilon^{tr})^{-1}$ is symmetric. If this is the case then the eigenvalues of $\mathbb{O}_d$ are purely real and our numerical scheme will not suffer from late time instabilities.

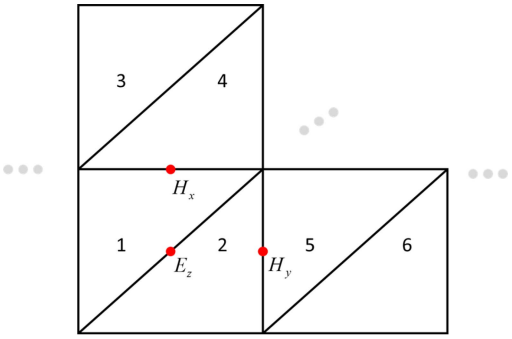

FIGURE 8. Yee cell and location of electric and magnetic displacement fields in the presence of triangular mesh.

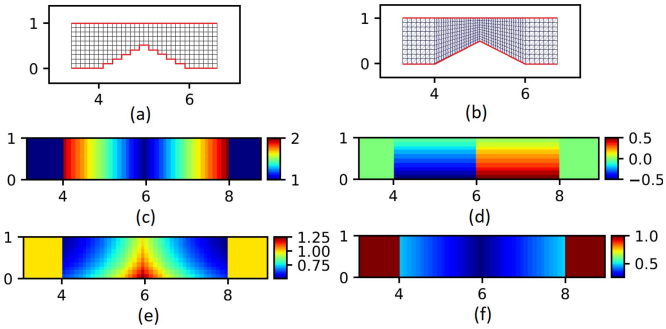

FIGURE 9. (a) and (b) meshing scheme for FDTD and the proposed method. (c), (d), (e) and (f) distribution of $\varepsilon_{xx}{}^{tr}$, $\varepsilon_{xy}{}^{tr}$, $\varepsilon_{yy}{}^{tr}$ and $\varepsilon_{zz}{}^{tr}$ for the lower section of each mesh cell in the proposed method, respectively.

D. SYMMETRIC IMPLEMENTATION OF ε^{TR-1} IN YEE CELL FOR A TRIANGULAR MESH

Eq. (9) and [32] shows that to create a stable FDTD algorithm we must find a Hermitian matrix that approximates (to second order) ε^{tr} and μ^{tr}. Consider, a two dimensional Yee cell, is shown in Fig. 8, for the transverse electric (TE) case. Here the red points indicate where the FDTD algorithm calculates the electric or magnetic fields and so indicates the points were we need approximations for the material parameters. Comparing Fig. 8 and Fig. 6 we can see that our transformation T is discontinuous at precisely the points where we need to calculate the fields and so some care is needed to properly symmetrise the relevant tenors. Therefore, our approach is to average over areas 1 and 2 of Fig. 8 for ε_{zz}. For the permeability, it should be averaged over 4 and 1 for μ_{xx}, 2 and 5 for μ_{yy} and finally 1, 2, 4 and 5 for both μ_{xy} and μ_{yx}. With this procedure the material tensors remain symmetric and we can thus avoid spurious instabilities in our simulations. To demonstrate this we turn to a couple of examples which also demonstrate the improvement in speed and accuracy of our method.

E. CFL STABILITY CONDITION

As the resulted relative permittivity and permeability in the transformed space may be smaller than unity, the speed of wave propagation can increase beyond the speed of light. In such a case, the wave can propagate more than one spatial step during a temporal step and this will lead into a numerical instability. This constraint is known as Courant-Friedrichs-Lewy (CFL) condition. In the previous researches [26]–[30], they have used dispersive materials to overcome this issue by the cost of adding unwanted frequency dependency on the simulation. However, an additional homogeneous anisotropic contraction of coordinate system in the transformed space can increase the amount of transformed permittivity and permeability in a way to satisfy the CFL condition [37].

III. RESULTS AND DISCUSSION

In order to demonstrate the superiority and implementation of our method we discuss here a couple of simple examples and compare the results of our method with a traditional FDTD algorithm, a simple transform optics based approach and finally a finite element approach using the commercial software package COMSOL.

Consider a waveguide with a discontinuity which is shown in Fig. 10(a). Edges 1 and 2 are chosen to be a perfect electrical conductor and the waveguide is terminated with a perfect match layer (PML) at both ends. To ensure that the amount of reflection caused by the PML is less than $-80dB$ of the incident wave which reaches the PML boundaries, we applied a fine tuned impedance matched lossy anisotropic dielectric magnetic materials similar to Uni-axial Perfect Match Layer (UPML) [38]. The conventional FDTD and proposed method mesh, for this example, are showing in Fig. 9 (a) and (b), respectively, and the PEC boundaries are indicated by the red lines. As it can bee seen in Fig. 9 (a) the straight PEC boundaries in discontinuity are replaced by stairs shape boundaries due to the limitation of classical FDTD method. However the present method can easily follow the slope of discontinuity. The $\varepsilon_{xx}{}^{tr}$, $\varepsilon_{xy}{}^{tr}$, $\varepsilon_{yy}{}^{tr}$ and $\varepsilon_{zz}{}^{tr}$ distribution corresponding to lower triangles in each meshing cell of the proposed method are shown in Fig. 9 (c), (d), (e) and (f), respectively. It is noticeable that as the length of boundary discontinuity is larger than its corresponding straight lines in the proposed method we increase the number of meshing in this area by the method of Fig. 3 (a). This example can be considered as a very fair scenario for the classical and TO FDTD as we only have a stationery discontinuity in one of the exterior boundaries. However, the proposed method provides more accurate results.

We used TE^1 mode to excite this structure and calculated S^{11} using the following formula:

$$S^{1n}(f) = \frac{\mathcal{F}\left\{\int \left(E^{\perp}_{total} - E^{\perp}_{incident}\right) E^{\perp}_{n} dl\right\}}{\mathcal{F}\left\{\int E^{\perp}_{incident} E^{\perp}_{n} dl\right\}} \tag{10}$$

in which, $E^{\perp}_{total}$, $E^{\perp}_{incident}$ and $E^{\perp}_{n}$ are the perpendicular components of the total, incident and nth modal electric fields respectively. Both integrations are done along the source plane (line) which is indicated by the blue line in Fig. 10 (a) and $\mathcal{F}$ represents the Fourier transformation. The incident electric field is taken to be a summation of couple of Gaussian pulses with overall $FWHM = 150MHz$ and so by

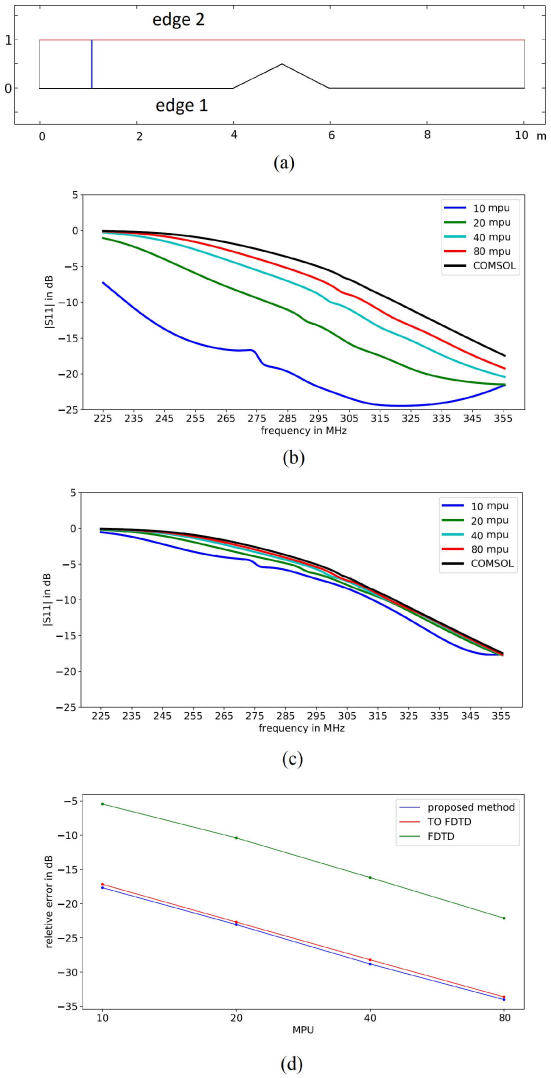

FIGURE 10. (a) geometry of waveguide. (b) S^{11} obtained from FDTD vs COMSOL. (c) calculated S11 using the proposed method vs COMSOL. (d) relative error.

taking the Fourier transform we can calculate the amount of reflected light in each mode at a particular frequency.

We calculated the S parameter for the proposed method, classical FDTD, TO FDTD and finally FEM via commercial software COMSOL. S^{11} obtained from classical FDTD vs COMSOL and proposed method vs COMSOL for the different number of meshing cells per unit length (MPU) is shown in Fig. 10. (b) and (c), respectively. We measure the accuracy of each method by integrating the error between it and the FEM solution over the upper and lower simulations' frequencies (f_1 and f_2), i.e.,

$$error = 10\log\left(\frac{\int_{f_1}^{f_2}\left(S^{11}_{comsol} - S^{11}\right)^2 df}{f_2 - f_1}\right) \qquad (11)$$

This measure for each method is shown in Fig. 10(d). As can be seen the proposed method is superior and results in almost an order of magnitude improvement compared to previous FDTD algorithms.

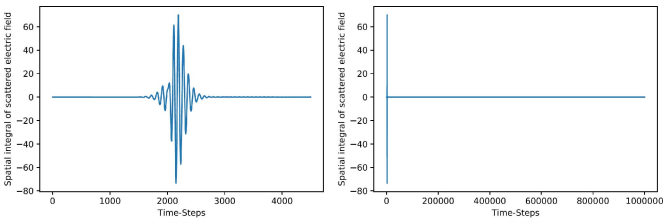

FIGURE 11. Spatial integral of scattered electric field over (a) 4500 time-steps (b) 1000000 time-steps obtained for the waveguide shown in Fig. 10 (a).

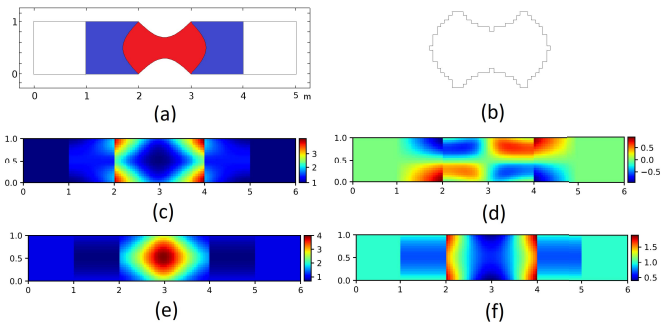

FIGURE 12. (a) Geometry of the waveguide. (b) approximated boundaries using uniform grid of classical FDTD. (c), (d), (e) and (f) $\varepsilon_{xx}{}^{tr}$, $\varepsilon_{xy}{}^{tr}$, $\varepsilon_{yy}{}^{tr}$ and $\varepsilon_{zz}{}^{tr}$ distribution.

To represent the results in the time domain, the numerator of the Eq. (10) ($\int (E^{\perp}_{total} - E^{\perp}_{incident}) E^{\perp}_{n} dl$) for 4500 and 1000000 time-steps is illustrated in Fig. 11(a) and (b), respectively. As it can be seen the simulation remains stable even after more than 1000 times of wave round trip over the waveguide structure.

The second example is waveguide with the internal and external boundaries discontinuities as shown in Fig. 12 (a). The area marked by the red colour in Fig. 12 is filled by a dielectric with permittivity equal to 2 in all range of simulation's frequency while the upper and lower edge are chosen to be PEC and the waveguide is terminated using PML at both ends. As before we excite the TE^1 mode using a short pulse and the S^{11} coefficient is calculated to investigate its behaviour. The meshing using our proposed method for the colored sections is shown in Fig. 4(b) while the approximated internal and external boundaries using a classical FDTD meshing scheme is shown in Fig. 12 (b). It is obvious that the conventional meshing scheme fails for both the internal and external boundaries and so the FDTD result will not be accurate when small MPU are chosen. Finally the purpose of the added white sections in Fig. 12 (a) is to relax the proposed mesh for the source and PML realization. The calculated $\varepsilon_{xx}{}^{tr}$, $\varepsilon_{xy}{}^{tr}$, $\varepsilon_{yy}{}^{tr}$ and $\varepsilon_{zz}{}^{tr}$ distribution in the transformed space based on the meshing scheme of Fig. 4(b) are shown in Fig. 12 (c), (d), (e) and (f), respectively. Please notice, as the curved external boundaries in the red section has a greater length than its corresponding straight line in the transformed space, like the previous example, we increased the number of meshing points on them, Fig. 4 (b).

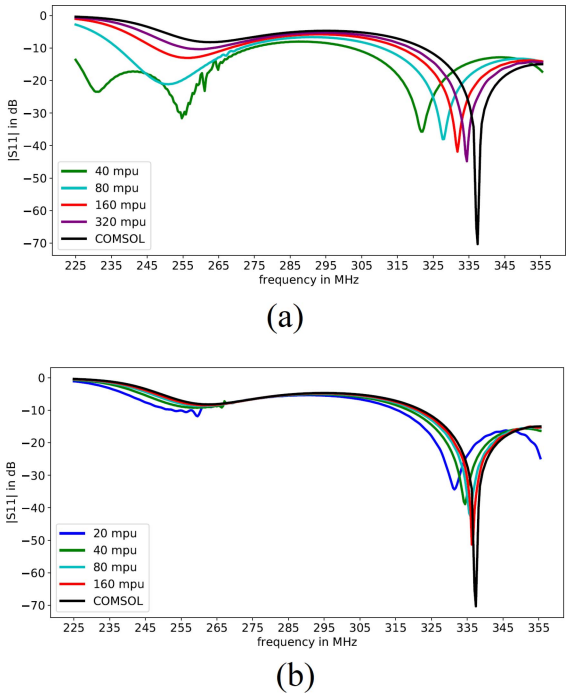

FIGURE 13. S^{11} **(a) FDTD (b) proposed method.**

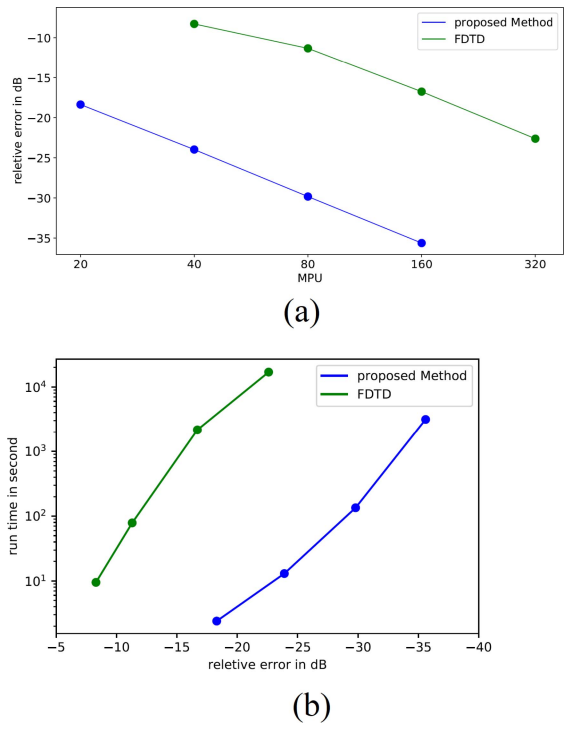

FIGURE 14. **(a) MPU vs relative error for FDTD and proposed method. (b) the relative error vs run time for FDTD and the proposed method.**

The resulted S^{11} from classical FDTD vs COMSOL and proposed method vs COMSOL is shown in Fig. 13(a) and (b), respectively. The detailed information about the total number of mesh cells and run times for each of the results using different MPU are shown in table (1), FDTD, and

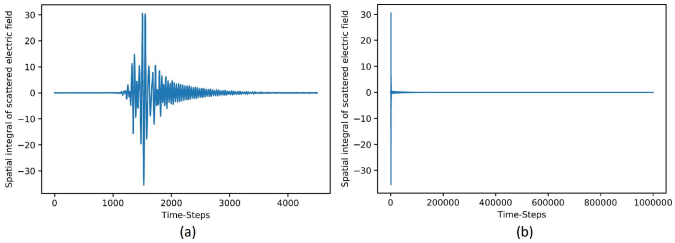

FIGURE 15. **Spatial integral of scattered electric field over (a) 4500 time-steps (b) 1000000 time-steps for the waveguide illustrated in Fig. 12(a).**

TABLE 1. **Total number of mesh, error and run time for FDTD.**

MPU	Total number of mesh	Error	Run time
40	19536	$-8.3dB$	$9.5s$
80	74256	$-11.3dB$	$78.7s$
160	289296	$-16.7dB$	$2164.3s$
320	1141776	$-22.6dB$	$16951.7s$

TABLE 2. **Total number of mesh, error and run time for the proposed method.**

MPU	Total number of mesh	Error	Run time
20	5856	$-18.3dB$	$2.4s$
40	21296	$-23.9dB$	$13.0s$
80	80976	$-29.8dB$	$134.7s$
160	315536	$-35.6dB$	$3143.0s$

table (2), proposed method. Results from the conventional FDTD using a MPU of 20 are not shown since it is too inaccurate while for our new method it falls in acceptable limits. Remarkably it can be seen that the proposed method gives more accurate results compared to the FDTD with eight times higher MPU. From Tables (1) and (2) two, this means around 1000 times faster computation when a specific amount of error is desired. The relative error vs MPU and the run time vs relative error for the proposed method and FDTD are shown in Fig. 14 (a) and (b), respectively.

The time domain results of the numerator of the Eq. (10) for 4500 and 1000000 time-steps is shown in Fig. 15(a) and (b), respectively. There is no sign of late-time instability even after more than 1000 wave round trips in the waveguide structure.

IV. CONCLUSION

A novel stable and accurate time-domain simulation technique based on a triangular meshing scheme and space curvature is developed. Firstly, a triangular gridding algorithm with the ability to follow any curved internal or external boundaries suitable for finite difference time domain (FDTD) methods is presented. Then we show that this new meshing can be transformed to a uniform grid using a local diffeomorphism. To keep the solutions of Maxwell's equations invariant under our transformation, we introduce anisotropic inhomogeneous material parameters and show how they can be calculated and used. Importantly our approach avoids inaccurate, nonphysical or late-time unstable

solutions present in other approaches. Finally we compare our present method against conventional FDTD and transformation optics FDTD algorithms using a couple of waveguide problems. We find that our method is at least one thousand times faster for the same level of accuracy when the problems deals with curved internal or external boundaries in a two dimensional simulation.

REFERENCES

[1] K. Yee, "Numerical solution of initial boundary value problems involving Maxwell's equations in isotropic media," *IEEE Trans. Antennas Propag.*, vol. 14, no. 3, pp. 302–307, May 1966.

[2] A. Taflove and M. E. Brodwin, "Numerical solution of steady-state electromagnetic scattering problems using the time-dependent Maxwell's equations," *IEEE Trans. Microw. Theory Techn.*, vol. 23, no. 8, pp. 623–630, Aug. 1975.

[3] A. Taflove, "Application of the finite-difference time-domain method to sinusoidal steady-state electromagnetic-penetration problems," *IEEE Trans. Electromagn. Compat.*, vol. EMC-22, no. 3, pp. 191–202, Aug. 1980.

[4] A. Taflove and S. C. Hagness, *Computational Electrodynamics: The Finite-Difference Time-Domain Method*. Boston, MA, USA: Artech House, 2005.

[5] I. S. Kim and W. J. Hoefer, "A local mesh refinement algorithm for the time domain-finite difference method using Maxwell's Curl equations," *IEEE Trans. Microw. Theory Techn.*, vol. 38, no. 6, pp. 812–815, Jun. 1990.

[6] D. T. Prescott and N. Shuley, "A method for incorporating different sized cells into the finite-difference time-domain analysis technique," *IEEE Microw. Guided Wave Lett.*, vol. 2, no. 11, pp. 434–436, Nov. 1992.

[7] W. Yu and R. Mittra, "A new subgridding method for the finite-difference time-domain (FDTD) algorithm," *Microw. Opt. Technol. Lett.*, vol. 21, no. 5, pp. 330–333, 1999.

[8] S. Wang, F. L. Teixeira, R. Lee, and J.-F. Lee, "Optimization of subgridding schemes for FDTD," *IEEE Microw. Wireless Compon. Lett.*, vol. 12, no. 6, pp. 223–225, Jun. 2002.

[9] I. Ahmed and Z. Chen, "A hybrid adi-FDTD subgridding scheme for efficient electromagnetic computation," *Int. J. Numer. Modell. Electron. Netw. Devices Fields*, vol. 17, no. 3, pp. 237–249, 2004.

[10] N. Marrone and R. Mittra, "A new stable hybrid three-dimensional finite difference time domain (FDTD) algorithm for analyzing complex structures," in *Proc. IEEE Antennas Propag. Soc. Symp.*, vol. 2, 2004, pp. 1680–1683.

[11] B. Donderici and F. L. Teixeira, "Improved FDTD subgridding algorithms via digital filtering and domain overriding," *IEEE Trans. Antennas Propag.*, vol. 53, no. 9, pp. 2938–2951, Sep. 2005.

[12] N. V. Venkatarayalu, R. Lee, Y.-B. Gan, and L.-W. Li, "A stable FDTD subgridding method based on finite element formulation with hanging variables," *IEEE Trans. Antennas Propag.*, vol. 55, no. 3, pp. 907–915, Mar. 2007.

[13] J.-P. Brenger, "A huygens subgridding for the FDTD method," *IEEE Trans. Antennas Propag.*, vol. 54, no. 12, pp. 3797–3804, Dec. 2006.

[14] J.-P. Bérenger, "The huygens subgridding for the numerical solution of the Maxwell equations," *J. Comput. Phys.*, vol. 230, no. 14, pp. 5635–5659, 2011.

[15] A. Zakharian, M. Brio, and J. V. Moloney, "FDTD based second-order accurate local mesh refinement method for Maxwell's equations in two space dimensions," *Commun. Math. Sci.*, vol. 2, no. 3, pp. 497–513, 2004.

[16] A. Zakharian, M. Brio, C. Dineen, and J. Moloney, "Stability of 2d FDTD algorithms with local mesh refinement for Maxwell's equations," *Commun. Math. Sci.*, vol. 4, no. 2, pp. 345–374, 2006.

[17] A.-T. Hayder, J.-P. Bérenger, and F. Costen, "Singularity problem with the one-sheet huygens subgridding method," *IEEE Trans. Electromagn. Compat.*, vol. 59, no. 3, pp. 992–995, Jun. 2017.

[18] J. M. Hyman, S. Li, P. Knupp, and M. Shashkov, "An algorithm for aligning a quadrilateral grid with internal boundaries," *J. Comput. Phys.*, vol. 163, no. 1, pp. 133–149, 2000.

[19] S. K. Khattri, "An adaptive quadrilateral mesh in curved domains," *Serdica J. Comput.*, vol. 3, no. 3, pp. 249–268, 2009.

[20] S. E. B. Boret and O. J. Jiménez. (2017). *Quadrilateral Grid Generation Supported on Complex Internal Boundaries Using Spectral Methods*. [Online]. Available: https://arxiv.org/abs/1712.07007

[21] R. Holland, "Finite-difference solution of Maxwell's equations in generalized nonorthogonal coordinates," *IEEE Trans. Nucl. Sci.*, vol. 30, no. 6, pp. 4589–4591, Dec. 1983.

[22] Z. Xie, C.-H. Chan, and B. Zhang, "An explicit fourth-order orthogonal curvilinear staggered-grid FDTD method for Maxwell's equations," *J. Comput. Phys.*, vol. 175, no. 2, pp. 739–763, 2002.

[23] Jin-fa-Lee, R. Palandech, and R. Mittra, "Modeling three-dimensional discontinuities in waveguides using nonorthogonal FDTD algorithm," *IEEE Trans. Microw. Theory Techn.*, vol. 40, no. 2, pp. 346–352, Feb. 1992.

[24] N. K. Madsen, "Divergence preserving discrete surface integral methods for Maxwell's curl equations using non-orthogonal unstructured grids," *J. Comput. Phys.*, vol. 119, no. 1, pp. 34–45, 1995.

[25] S. D. Gedney and J. A. Roden, "Numerical stability of nonorthogonal FDTD methods," *IEEE Trans. Antennas Propag.*, vol. 48, no. 2, pp. 231–239, Feb. 2000.

[26] J. Liu, M. Brio, and J. V. Moloney, "Transformation optics based local mesh refinement for solving Maxwell's equations," *J. Comput. Phys.*, vol. 258, pp. 359–370, Feb. 2014.

[27] R. Chen, L. Kuang, Z. Zheng, and Q. H. Liu, "Transformation optics-based finite difference time domain algorithm for scattering from object with thin dielectric coating," *IEEE Access*, vol. 7, pp. 150060–150071, 2019.

[28] J.-S. Hong, W.-M. Cheng, M.-C. Yang, R.-C. Shiu, Y.-C. Lan, and K.-R. Chen, "Enhancing efficiency of electromagnetic simulation in time domain with transformation optics," *Appl. Sci.*, vol. 8, no. 7, p. 1133, 2018.

[29] R. Chen, L. Kuang, P. Ren, and Q. H. Liu, "Modified transformation optics based FDTD for local mesh refinement," in *Proc. IEEE Progr. Electromag. Res. Symp. (PIERS)*, Toyama, Japan, 2018, pp. 1138–1140.

[30] R. Chen, L. Kuang, Z. Zheng, and Q. H. Liu, "A novel transformation optics-based FDTD algorithm for fast electromagnetic analysis of small structures in a large scope," *IEEE Access*, vol. 7, pp. 124750–124758, 2019.

[31] J. B. Pendry, D. Schurig, and D. R. Smith, "Controlling electromagnetic fields," *Science*, vol. 312, no. 5781, pp. 1780–1782, 2006.

[32] G. R. Werner and J. R. Cary, "A stable FDTD algorithm for non-diagonal, anisotropic dielectrics," *J. Comput. Phys.*, vol. 226, no. 1, pp. 1085–1101, 2007.

[33] A. F. Oskooi, C. Kottke, and S. G. Johnson, "Accurate finite-difference time-domain simulation of anisotropic media by subpixel smoothing," *Opt. Lett.*, vol. 34, no. 18, pp. 2778–2780, 2009.

[34] G. R. Werner, C. A. Bauer, and J. R. Cary, "A more accurate, stable, FDTD algorithm for electromagnetics in anisotropic dielectrics," *J. Comput. Phys.*, vol. 255, pp. 436–455, Dec. 2013.

[35] R. Courant, K. Friedrichs, and H. Lewy, "Über die partiellen differenzengleichungen der mathematischen physik," *Mathematische Annalen*, vol. 100, no. 1, pp. 32–74, 1928.

[36] A. C. Cangellaris and D. B. Wright, "Analysis of the numerical error caused by the stair-stepped approximation of a conducting boundary in FDTD simulations of electromagnetic phenomena," *IEEE Trans. Antennas Propag.*, vol. 39, no. 10, pp. 1518–1525, Oct. 1991.

[37] M. Kazemzadeh, W. Xu, and N. G. R. Broderick, "Faster and more accurate time domain electromagnetic simulation using space transformation," *IEEE Photon. J.*, vol. 12, no. 4, pp. 1–13, Aug. 2020.

[38] S. D. Gedney, "An anisotropic perfectly matched layer-absorbing medium for the truncation of FDTD lattices," *IEEE Trans. Antennas Propag.*, vol. 44, no. 12, pp. 1630–1639, Dec. 1996.